IEEE Access
Multidisciplinary | Rapid Review | Open Access Journal

Date of publication xxxx 00, 0000, date of current version xxxx 00, 0000.

Digital Object Identifier 10.1109/ACCESS.2024.0429000

Mobility-Aware Bivariate Line-of-Sight Probability for Air-to-Ground Communications Using Millimeter and Terahertz Waves

BASHEER AMEEN RADDWAN[1], IBRAHIM AHMED AL-BALTAH[1,2]
[1]Department of Information Technology, Faculty of Computer Science and IT, Sana'a University, Sana'a, Yemen (e-mail: basheer@su.edu.ye)
[2]Department of Information Technology, Faculty of Science and Engineering, Al-Hikma University, Sana'a, Yemen

Corresponding author: Basheer Ameen Raddwan (e-mail: basheer@su.edu.ye).

ABSTRACT This paper presents a mobility-aware bivariate line-of-sight (LoS) probability model for millimeter waves and terahertz air-to-ground communication. Current literature does not provide LoS models that consider using directional antennas on the unmanned aerial vehicle that acts as an air base station (airBS). Furthermore, in the context of having large stationary blockers, the impact of ground user terminals' (gUTs) and airBSs' mobility remains unexplored. To simulate the ray-tracing between gUTs and airBSs in both scenarios where the airBSs have omnidirectional or directional antennas, we develop a game engine-based synthetic urban layout generator. We analyze ray-tracing as a bivariate probability and formulated a unified joint probability function that could predict the LoS probability for omnidirectional and directional scenarios. The proposed model outperformed the existing models in the omnidirectional scenario. We also present a benchmark for the model's performance in the directional scenario. Moreover, using ray-tracing simulation, we examine the influence of mobility on the service time, also known as the sojourn time, and developed two cubic polynomial models to forecast the service time for any urban layout that aligns with the ITU-R P.1410-5 build-up parameters.

INDEX TERMS Line-of-Sight probability, mobility, air-to-ground communication, multi-Access edge Computing, ray-tracing, unmanned aerial vehicles, service time, sojourn time, urban, simulation

I. INTRODUCTION

THE advent of unmanned aerial vehicles (UAVs) in the last several years has varied its uses in fifth-generation (5G) and future technologies, thanks to their reputation for low operating costs and impressive mobility. To improve coverage in high-traffic regions or areas hit by natural catastrophes, UAVs serve as air relays or base stations (airBSs). In addition, there has been a recent uptick in the practice of using UAVs equipped with computing power or storage capacity to accomplish higher data throughput or real-time services in fog computing and multi-access edge computing (MEC), particularly when employing high frequencies like terahertz and millimeter waves (mm-waves) [1], [2].

In addition to the various uses previously mentioned, UAVs acting as airBSs can provide superior line-of-sight (LoS) conditions with ground user terminals (gUTs) compared to ground base stations. The LoS conditions improve radio communication capacity and performance in various communication channels, such as air-to-ground (A2G) and ground-to-air (G2A). The LoS probability, P_{LoS}, estimates the LoS condition that ranges from zero to one, where zero means non-LoS (NLoS) and one means the existing direct sight condition, LoS. In addition, the P_{LoS} is an indispensable part of communication channel modeling, which is essential for network planning and optimization [3].

A. BRIEF REVIEW OF P_{LOS} MODELS

Standard body organizations and academic researchers have made numerous attempts to model the P_{LoS}. For the standard effort, the International Telecommunication Union (ITU) introduced two models: the general one, presented in [4], and the cellular-based one, known as M.2135 [5]. Both are based on ground-to-ground (G2G) communication channels. Another two standards, WINNER-II [6] and 3GPP TR 38.900 [7], took a similar approach to the M.2135. They both focus on the urban micro (UMi) and urban macro (UMa) cell scenarios. More models were presented for the G2G communication channels from the academic research such as [8]–[12].

The emergence of different use cases for UAVs has motivated new communication channel models and, consequently,

TABLE 1. Comparison of existing LoS probability models for large stationary blockages.

Reference	Approach	Ray-tracing	Channel	Building locations	Building height	Variables	ITU	Variance	Directional LoS	Mobility
[4]	Statistical	×	G2G	1D-even	Rayleigh	(x, y)	✓	univariate	×	×
[13]	Empirical	×	A2G	1D-even	Rayleigh	(θ)	×	univariate	×	×
[14]	Empirical	×	A2G	1D-PPP	Rayleigh	(θ)	✓	univariate	×	×
[8]	Geometry	×	G2G	2D-PPP	-	(x)	×	univariate	×	×
[7]	Empirical	×	G2G	1D-even	Rayleigh	(x)	×	univariate	×	✓
[10]	Geometry	×	G2G	1D-HPPP	Rayleigh	(x)	×	univariate	×	×
[11]	Geometry	×	G2G	2D-HPPP	Uniform	(f_c)	×	univariate	×	×
[15]	Statistical	✓	A2A	2D-PPP	Rayleigh	(h_{rx}, θ)	✓	univariate	×	×
[16]	Statistical	×	A2G	1D-IPPP	Rayleigh	(x, y)	✓	univariate	×	×
[17]	Statistical	✓	A2G	2D-PPP	Log-Normal	(x, y)	×	univariate	×	×
[12]	Geometry	×	G2G	1D-HPPP	Rayleigh	(f_c)	×	univariate	×	×
[18]	Geometry	×	G2A	MPLP	Rayleigh	(x)	×	univariate	×	×
[19]	Geometry	×	S2G	1D-even	Rayleigh	(θ)	×	univariate	×	×
[20]	Geometry	×	A2G	1D-even	Rayleigh	(x)	×	univariate	×	×
[21]	Geometry	×	A2G	Grid	Rayleigh	(x, y)	✓	univariate	×	×
[22]	Machine Learning	✓	A2G	1D-PPP	Rayleigh	(y)	×	univariate	×	×
[23]	Statistical	✓	A2G	Grid	Rayleigh	(θ)	×	univariate	×	×
[24]	Integral Geometry	×	G2A	2D-Uniform	Uniform	-	×	univariate	×	×
[25]	Geometry	×	A2G	2D-Uniform	Rayleigh	(θ)	✓	univariate	×	×
[26]	Statistical	✓	A2G	Grid	Rayleigh	(θ)	✓	univariate	×	×
[27]	Machine Learning	×	A2G	1D-PPP	Rayleigh	(θ)	×	univariate	×	×
[28]	Statistical	✓	A2G	Grid	Rayleigh	(x, y)	✓	univariate	×	×
[29]	Geometry	×	A2G	Grid	Rayleigh	(θ, w_b, w_s)	✓	univariate	×	×
[30]	Empirical	×	S2G	-	-	(θ, ϕ)	×	univariate	✓	×
This article	Statistical	✓	A2G	Grid	Rayleigh	(x, y)	✓	Bivariate	✓	✓

new P_{LoS} models, such as air-to-ground (A2G) [13], [14], [16], [17], [20]–[23], [25]–[29], ground-to-air (G2A) [18], [24], air-to-air (A2A) [15], and satellite-to-ground (S2G) [19], [30]. We compiled and compared existing models in Table 1. The table divides existing models into different groups based on the modeling approach, communication channel type, building location and height distribution, input variables, ITU-R compatibility of the urban layouts [4], the variance of input random variables, supporting directional antennas in the P_{LoS} models, and supporting mobility.

Existing models present four modeling approaches: empirical, geometrical, statistical, and machine learning. The empirical models are formulated from real-world measurement or simulation data. These models target specific urban layouts. The geometry-based models are formulated by estimating the LoS condition from the geometry arrangement of objects in the environments. For example, [18] assumed the ground base stations are located in the cross-section of roads, while [29] assumed a special environment that can be divided into four blocks or quarters. Machine learning LoS models are created by training classification algorithms for predicting the LoS condition. The statistic models are formulated by analyzing the results of stochastic geometry or stochastic sampling of the environment, which are collected in real-world environments or by ray-tracing simulation of three-dimensional (3D) digital urban layouts.

Every modeling approach has its advantages and disadvantages. For example, the empirical approach can have high prediction accuracy, but it is time-consuming and requires notable human force and equipment for collecting data. While the geometry-based approach is suitable for general models, it necessitates additional calculations to determine the arrangement of urban layouts and the relative positions of communication nodes within those layouts. The machine learning models need real-world or simulation data, which makes implementation a challenging task. Moreover, current literature does not provide an open-source, ready-to-use trained model, and the researcher has to build everything from scratch. Because the statistical approaches rely on real-world data or ray-tracing simulations, they are also known as the deterministic approach. It can produce accurate models but has a high overall cost for collecting real-world data, whereas ray-tracing simulations have a high computational complexity [31].

Different distribution schemes for building location and height appear to play an important role in LoS probability modeling. Buildings are distributed along the line that connects the transmitter with the receiver as one-dimensional evenly spaced (1D-even) [4], [7], [13], [19], [20], 1D Poisson Point Process (1D-PPP) [14], [22], [27], 1D inhomogeneous PPP (1D-IPPP) [16], and 1D homogeneous PPP (1D-HPPP) [10], [12]. The two-dimensional (2D) distribution of buildings is studied using grid distribution [21], [23], [26], [28], [29], Manhattan Poisson Line Process (MPLP) [18], 2D-PPP

[8], [15], [17], 2D-HPPP [11], and 2D-uniform [24], [25]. In addition, the Rayleigh distribution is used in most of the previous work to distribute the height of buildings, except for a few works that used uniform [11], [24] and log-normal [17] distributions. The ITU-R P.1410-5 [4] models urban layouts using three parameters, also known as the build-up parameters. The literature commonly classifies models as ITU or non-ITU to indicate that the ITU is following the build-up parameters model. In the urban layout model Section II-A, we will describe the ITU build-up parameters and other ITU-related aspects.

B. LIMITATIONS OF THE EXISTING MODELS

Let us denote the horizontal ground distance between transmitter and receiver as x, the altitude difference between them as y, the elevation angle of the ray that connects them as θ, and the center frequency as f_c. The rest of the symbols used in the variable column in Table 1 are defined in Table 2 in Section II. We analyze the existing models and found that most of them input x, y, and θ as a single variable or two variables as (x, y). Although several models input two variables, none have defined the LoS probability as a multivariate or bivariate probability. We believe that modeling the P_{LoS} as a multivariate or bivariate probability function can enhance the prediction accuracy of the model because of the probable better scoping of the variables.

Using directional antennas is a common practice in wireless networks [32] because it improves the overall signal-to-interference-plus-noise ratio (SINR). Deploying an airBS with an omnidirectional antenna to an altitude of 100 meters, for example, could create a line-of-sight condition with a large number of gUTs over a long distance, which in turn interferes with those gUTs we do not want the airBS to cover, affecting the overall performance of the network. Using directional antennas on airBSs can help to reduce that unwanted interference. Figure 1 shows that the LoS when using a directional antenna is a subset of the LoS when using an omnidirectional antenna. For instance, if the airBS is equipped with an omnidirectional antenna, users B, C, and D are in the line-of-sight. In contrast, if the airBS is equipped with a directional antenna, only user B is in line-of-sight with the airBS because its location is within the coverage of the main lobe of the airBS's directional antenna. As a result, the airBS's interference does not impact users A, C, and D. However, none of the existing LoS models cater to the directional antenna scenario for the A2G communication in environments with large stationary blockers.

In normal real-world scenarios, both gUTs and airBSs are likely to be in mobile status. Few studies have considered the mobility of objects in the context of studying dynamic small blockage [33]–[35]. The study [7] introduced the soft LoS model to model the transition from LoS state to the NLoS state for the G2G communication channels. mobility-aware modeling of LoS probability is still an opportunity in the A2G communication channels, especially in large stationary blockages, like buildings. The mobility of the gUT and the

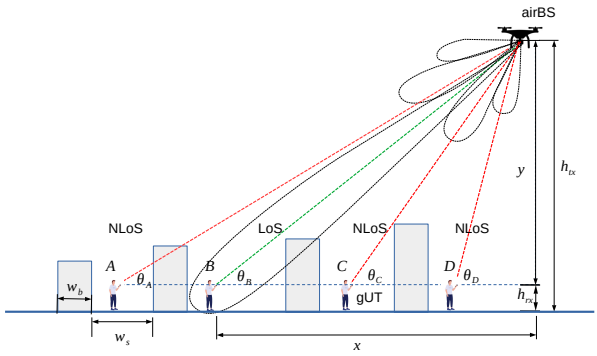

FIGURE 1. An airBS that uses a directional antenna can be in line-of-sight with a gUT only if the gUT is located within the coverage of the antenna's main lobe.

airBS is a challenge, not only in communication channel modeling [32], but also in planning dynamic resources for latency-sensitive task offloading to the MEC [36]. Planning where to deploy the MEC datacenters and their resources requires an environment-dependent model that could estimate the average connecting time between a gUT and an airBS. The connecting time is usually known as the service time or the sojourn time. This refers to the average time a gUT spends in the LoS state when connected to an airBS. The current literature lacks environment-dependent service time models, which are critical for MEC-assisted wireless network planning.

Moreover, current works examine the influence of mobility on handover primarily via handover rate, handover probability, and sojourn duration. Only a few studies have taken into account mobility in A2G communication systems. [37] studied the handover probability in a drone cellular network, while [38] studied the handover rate and the sojourn time. The stochastic approach is usually followed in modeling the sojourn time, as in [37], [38], but mobility tracing is also used [39]. The stochastic approach does not consider the environmental impact, whereas the mobility tracing method is less cost-effective and describes specific environments. In this study, we introduce an environment-dependent sojourn time model, which we empirically develop from the ray-tracing simulation.

To depict real-world datasets, the ray-tracing simulation is used in [17], [23], and [26]. Few datasets are there, such as the City of Melbourne Open Data [40], New York City Open Data [41] or at least the build-up parameters like Cologne City, Germany [29]. To simplify the LoS probability modeling process, it requires additional datasets or an alternative approach to real-world datasets. To solve such problems, geometry-based models [18], [28], [29] have been introduced; however, using synthetic digital urban layouts can not only reduce the ray-tracing simulation complexity but also provide a systematic study of the LoS probability in a large number

of urban layouts.

C. KEY CONTRIBUTIONS

- **Mobility-Aware Synthetic Urban Layout Generator**: We develop a synthetic urban layout generator for ray-tracing simulation of any ITU-R P.1410-5 build-up parameter combination. We employ game-engine advancements to reduce the complexity of 3D graphics computation and ensure seamless calculation of object transformations and ray-tracing to generate mobility-enabled arbitrary 3D synthetic urban layouts. We simulate ray-tracing for mobile gUTs and mobile airBSs, whereas existing models do not. One benefit of using mobile network elements is the ability to generate human-like outdoor position distribution with a minimum number of gUTs. The second is to know the average time between handovers, which is important to determine the best placement of cloud computing extensions, such as fog computing and MEC. The code of the generator is called Panda5gSim and is available on GitHub [42].
- **Unified Bivariate P_{LoS} model**: We present a complete, unified 3D A2G statistical-based LoS probability model that can predict the LoS probability no matter what type of antenna the airBS chooses. The proposed model, P_{LoS}, accepts two fitting parameters. For each parameter, we provide two cubic functions, one for the omnidirectional antenna scenario and the other for the directional antenna scenario. Each fitting function is varied with one variable that represents the urban environment; we call it the urban layout complex argument. More about the complex argument formulation is described in the urban layout model, Section II-A.
- **Two Service Time Models**: From the network designer's perspective, it is important to know how long a mobile gUT can stay in LoS condition with a mobile airBS in different urban layouts to determine what kind of MEC services can be provided and what resources are required to provide a specific service. For example, to provide off-loading service to the MEC for one Giga-Byte average task size, it is important to know the average service time to calculate where to locate the MEC and what MIMO (multi-input, multi-output) configuration is required in the airBS antenna. The service time, also known as sojourn time, is important for service-aware network design, especially for time-sensitive services that are hosted in fog or MEC data centers. Here we propose two polynomial environment-dependent service time models; one for the omnidirectional and the other for the directional scenarios.
- **Deeper Performance Analysis**: The ITU-R can represent an urban layout using three parameters (α, β, γ), while [14] introduced a 2D representation of $(\alpha\beta, \gamma)$. The two representations cannot provide a simple environment-dependent comparison of models, which is important for analyzing models' generality. To solve this problem, we introduce a single variable representation of urban layouts that we call the complex argument of the urban layout, as we formulate in Section II-A. The complex argument $(\mathcal{E})$ enables a comprehensive analysis of the model's performance overall in the ITU-R range of urban layouts. Moreover, in mm-wave and terahertz contexts, the LoS probability is more likely to represent a binary classification of LoS and NLoS conditions. We expand the generality analysis to include some binary classification metrics and investigate the probable bias of the models' performance.

The rest of this article presents the system model in Section II, which contains the urban layout model, the network model, the mobility model, the P_{LoS} model, and the service time model. In Section III, we describe the proposed mobility-aware ray-tracing simulation including the the 3D synthetic urban layout generator and simulation setup. The results are reported in Section IV, which describes the data balancing process, results of omnidirectional and directional scenarios, and generality analysis. We benchmark the performance of the proposed directional P_{LoS} model and the service time models. The limitations and future work are described in Section V while the conclusion is in Section VI.

II. THE SYSTEM MODEL

This section describes the system model which includes the urban layout model, the network model, the mobility model, the bivariate LoS probability model, and the service time model. The definitions of symbols used in the models are listed in Table 2.

A. THE URBAN LAYOUT MODEL

The ITU-R P.1410-5 [4] has introduced three parameters to describe any urban layout. These parameters are also known as the build-up parameters, which are α, β, and γ. The α [dimensionless] is the ratio of built-up area to the total area. The β [buildings/km^2] is the number of buildings in a square kilometer, while the γ [meters] is the mode of the Rayleigh distribution that describes the height of buildings. The α is defined from 0.1 for suburban to 0.8 for dense urban. Similarly, the β is defined from 750 to 100, while the γ is defined from 8 meters for suburban to 50 meters for high-rise urban.

For any arbitrary urban layout, the α can be calculated by dividing the summation of areas of buildings' polygons by the total area. The β can be calculated by (1), where N_{poly} is the number of polygons in the map of the area while $\mathbb{A}$ is the total area in square kilometers.

$$\beta = \frac{N_{poly}}{\mathbb{A}}. \tag{1}$$

The γ can be calculated from the mean property of the Rayleigh distribution. For example, if an arbitrary urban layout has a mean height of buildings $E(H_B)$ [meters], the γ

TABLE 2. Definitions of symbols used in the model.

Symbol	Unit	Definition
α	-	Ratio of built-up area to the total area
β	Buildings/ km^2	Number of buildings in a square kilometer
γ	m	Rayleigh mode parameter determining the building height
N_{poly}	-	Number of buildings' polygons on the area's map
$\mathbb{A}$	km^2	Total area
w_b	m	Width of building
w_s	m	Width of street
$\mathcal{E}_c$	-	Complex representation of urban layout
$\mathcal{E}$	radian	Complex argument representation of urban layout
N_{airBS}	-	Number of airBSs
N_{gUT}	-	Number of gUTs
ϕ	radian	Azimuth angle of the ray connecting an airBS with a gUT
θ	radian	Elevation angle of the ray connecting an airBS with a gUT
θ_{3dB}	degree	Vertical 3 dB beamwidth of a directional antenna
ϕ_{3dB}	degree	Horizontal 3 dB beamwidth of a directional antenna
$\mathcal{V}_{airBS}$	m/s	Velocity of airBS
$\mathcal{V}_{gUT}$	m/s	Velocity of gUT
x	m	Horizontal ground distance between airBS and gUT
y	m	Altitude difference between airBS and gUT
X	m	Continues random variable of ground distance
Y	m	Continues random variable of altitude difference
$\mathbf{A}$	-	Area of bivariate double integral
$f(\cdot)$	-	Probability distribution function (PDF)
$F(\cdot)$	-	Cumulative distribution function (CDF)
P_{LoS}	-	LoS probability ($F(\cdot)$)
$f_X(\cdot)$	-	PDF of marginal function in x direction
$f_Y(\cdot)$	-	PDF of marginal function in y direction
$F_X()$, $F_Y()$	-	CDF of $f_X()$ and $f_Y()$, respectively
$f(x\|y)$	-	Conditional PDF in x direction where $Y \leq y$
$f(y\|x)$	-	Conditional PDF in y direction where $X \leq x$
$F(x\|y)$, $F(y\|x)$	-	CDF of $f(x\|y)$ and $f(y\|x)$, respectively
$F_m(x,y)$	-	Joint probability matrix of ray-tracing
$f(x,y)$	-	Joint PDF function
$F(x,y)$	-	Joint CDF function
a, b	-	Fitting parameters
$\mathcal{T}$	s	Service time (aka sojourn time)

is determined by (2) where H_B is the random variable of building's height.

$$\gamma = \sqrt{\frac{2}{\pi}} E(H_B). \tag{2}$$

The density of buildings in a unit area is determined by $\alpha\beta$ [buildings/km^2]. Additionally, the width of the building and the width of the street are expressed in (3) and (4), respectively.

$$w_b = 1000\sqrt{\alpha/\beta}. \tag{3}$$

$$w_s = \frac{1000}{\sqrt{\beta}} - w_b. \tag{4}$$

The work in [14] reduced the representation of urban layout from three parameters in [4] to two parameters, which are the density of building in a square kilometer, denoted by $\alpha\beta$, and the γ. We simplify that by using a complex representation of the urban layout, as expressed in (5).

$$\mathcal{E}_c = (w_s - w_b) + i(w_s - \gamma), \tag{5}$$

where $\mathcal{E}_c$ is a complex representation of an arbitrary urban layout as a function of direct and indirect ITU-R build-up parameters. The expression in (5) is simplified to the complex argument $\mathcal{E}$ [radians] as in (6) to provide a single variable representation of that urban layout.

$$\mathcal{E} = \arg(\Im(\mathcal{E}_c), \Re(\mathcal{E}_c)), \tag{6}$$

where $\Re(\cdot)$ and $\Im(\cdot)$ are the real and imaginary parts of the complex representation. The $\mathcal{E}$ is uniquely defined in the range $[-\pi, \pi]$ for any combination of α, β, γ in the defined ranges of ITU-R.

Figure 2 illustrates the distribution of the urban layout complex argument for the four standard layouts as angles around a unit circle. The complex argument in the figure is represented by the angle of each point and measured in degree to ease the reading, while the later calculation always uses radians. The numerical values are presented in Table 3, which sorts the standard urban layouts according to the ascending value of $\mathcal{E}$. The advantage of the complex argument representation is shown clearly in the result discussion (see Section IV) where the comparison between models over a large number of urban layouts becomes easier with simple line plotting.

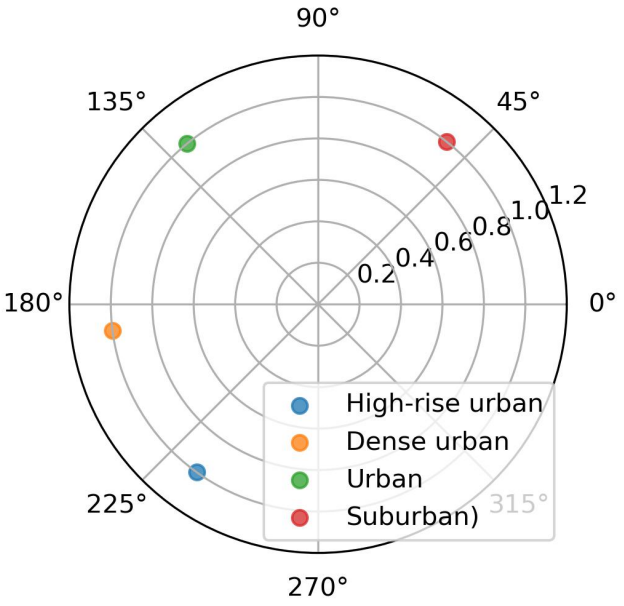

FIGURE 2. Polar visualization of the four standard urban layouts using the complex argument as expressed in (6).

B. THE NETWORK MODEL

After we generate the synthetic urban layouts as described in the previous section, we generate the network elements

TABLE 3. An example of standard urban layouts.

Environment	α	β	γ	$\alpha\beta$	$\mathcal{E}$
Dense Urban	0.5	300	20	150	-3.01
High-rise Urban	0.5	300	50	150	-2.20
Suburban	0.1	750	8	75	0.90
Urban	0.3	500	15	150	2.26

(NEs) that represent the transmitters on the airBSs and the receivers on the ground user terminals. Assume we have several airBSs that is denoted by N_{airBS} and several gUTs that is denoted by N_{gUT}. For any pair of an airBS and a gUT, we can describe the locations of these NEs using a global coordinate system (GCS) or a local coordinate system (LCS). The GCS provides NEs' relative location and direction to the environment's origin point. The LCS provides the relative location and direction of the gUT as observed from the airBS, taking into account that the origin of the LSC is the center point of the airBS, and the direction of the x-axis also aligns with the direction of the airBS.

Let's assume that the gUTs are equipped with omnidirectional antennas, while the airBSs operate in two different scenarios: the first uses omnidirectional antennas, and the second uses directional antennas. For an omnidirectional scenario, we use the transformation of a NE to determine the direct 3D distance d, horizontal ground distance x, and altitude difference y between any two NEs in the GCS. Let G_{airBS} be the omnidirectional antenna gain, with a constant value in all directions around the antenna.

One major issue of using directional antennas is the need to determine the antenna gain in the specific direction of the gUT. The relative transformation of the gUT to the airBS is determined according to the LCS of the airBS coordinate system. That relative transformation contains the position and Euler's transformation angles that translate the GCS into the LCS coordinate system, including horizontal ground distance x, altitude difference y, elevation angle θ, azimuth angle ϕ, and slant angle ψ. The conversion between coordinate systems in this article follows 3GPP TR 38.900, section 7. We use the 3GPP directional antenna, as modeled in 3GPP TR 38.900 table 7.3-1. The radiation pattern of the 3GPP antenna is shown in Figure 3, where the vertical 3 dB beamwidth θ_{3dB} and the horizontal 3 dB beamwidth ϕ_{3dB} are set to 65^o. As a result, the 3GPP directional antenna's maximum radiation power is 8 dBi. For more information on GCS, LCS, and 3GPP antennas, refer to [7].

C. THE MOBILITY MODEL

We assume that all NEs have the mobile capability, and the average movement velocities are denoted by $\mathcal{V}_{airBS}$ and $\mathcal{V}_{gUT}$ for airBS and gUT, respectively. To enable the autonomous movement of NEs, we generate a navigation mesh for every urban layout based on the widths of buildings and streets. The navigation mesh is a 2D polygonal representation of a 3D urban layout that enables gUTs and airBSs to effectively navigate around buildings. Games and other interactive simulations commonly use this technique to enable agents to find paths from one point to another while avoiding collisions. A grid-like navigation mesh is used, with a step size calculated by rounding the $\frac{\sqrt{\mathbb{A}}}{w_b+w_s}$. The star algorithm uses the navigation mesh to determine the shortest path from the source point to the destination point of movement. We randomly select the source and destination mobility points from the navigation mesh grid points.

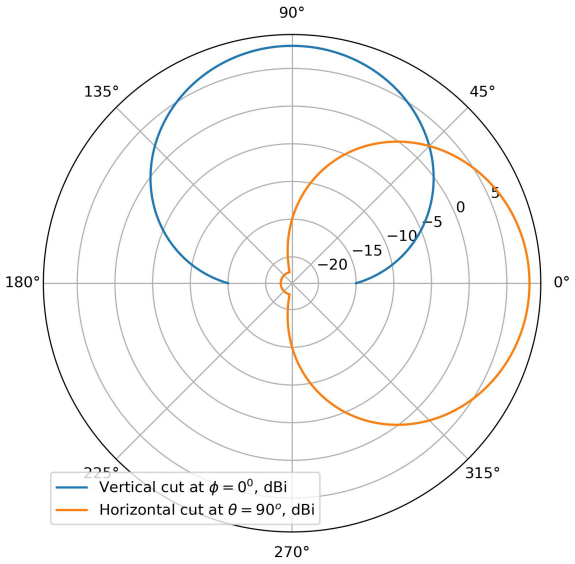

FIGURE 3. Single element radiation pattern of the 3GPP TR 38.900 directional antenna.

The mobility pattern resembles that of human movement. When the NE receives its target, it begins to move along the selected shortest trajectory. After the NE arrives at the target, it stays for a randomly generated time. Once the stay period concludes, the mobility manager assigns a new target to continue the pattern. We select a short stay time, with an average of one second, to ensure that all NEs remain mobile for the majority of the simulation time.

D. THE BIVARIATE P_{LOS} MODEL

We assume that the probability of having a line-of-sight condition between a transmitter on an airBS and a receiver on a gUT can be approximated by a joint distribution of (X, Y), which can be described by a non-negative joint probability density function $f(x, y)$ for a subset area $\mathbf{A} \in \mathbb{R}^2$. The probability $P_{LoS}((X, Y) \in \mathbf{A})$ is expressed by (7), where X and Y are continuous random variables that represent the ground distance and height difference between the airBS and the gUT, respectively.

$$P((X, Y) \in \mathbf{A}) = \iint_{\mathbf{A}} f(x, y)dxdy \tag{7}$$

where

$$\iint_{\mathbb{R}^2} f(x, y)dxdy = 1 \tag{8}$$

The cumulative distribution function (CDF) for a random vector (X, Y) is denoted by $F(x, y)$ and defined as

$$F(x, y) \doteq P(X \leq x, Y \leq y) \tag{9}$$

for $x, y \in \mathbb{R}$.

Then, the $P_{LoS}(x, y)$ is approximated as expressed in (10).

$$P_{LoS}(x, y) = F(x, y) = \int_{-\infty}^{x} \int_{-\infty}^{y} f(u, v) du dv. \tag{10}$$

We need to empirically determine whether the variables X and Y are independent to find $f_X(x)$ and $f_Y(y)$, which represent the univariate marginal PDF functions of both variables, respectively. In the case of dependent variables, the joint PDF function would be a multiplication of $f_X(x)$ and $f_Y(y)$, while in the independent case, the marginal functions are calculated as a conditional probability as in (11) and (12).

$$F(x|y) = \int_{-\infty}^{x} \frac{f(u, v)}{f_Y(y)} du. \tag{11}$$

$$F(y|x) = \int_{-\infty}^{y} \frac{f(u, v)}{f_X(x)} dv. \tag{12}$$

Therefore, the $P_{LoS}(x, y)$ probability model is expressed based on (10), (11), and (12) as in (13).

$$P_{LoS}(x, y) = \int_{-\infty}^{x} \int_{-\infty}^{y} f(u|v) f(v|x) du dv, \tag{13}$$

where $f(x|y)$ and $f(y|x)$ are the derivatives of $F(x|y)$ in x direction and $F(y|x)$ in y direction, respectively.

E. SERVICE TIME MODEL

Unlike the previous models, which evaluated the P_{LoS} with stationary NEs, this work focuses on the mobility effect on the positive LoS condition. We are aware that the mobility patterns may not contribute to the P_{LoS} model; however, the mobility can severely impact the communication channel if the line-of-sight is lost. As a result, we believe that modeling service time using the same approach as modeling the P_{LoS} is essential for network design and resource allocation in wireless networks and MEC-assisted networks.

To model the service time (sojourn time), denoted by $\mathcal{T}$, we run the mobility simulation for a period that we call the simulation time and collect the ray-tracing conditions and transformations every second. To determine which i-th airBS is serving the j-th gUT, we estimate the SINR and connect the gUTs to the airBSs based on the best SINR. To do that, we calculate the path loss PL [dB] as in (14).

$$PL = \begin{cases} FSPL, \ if \ \ LoS \\ FSPL + A_B, \ if \ \ NLoS, \end{cases} \tag{14}$$

where $FSPL = 20\log(d) + 20\log(f_c) - 27.55$ is the free space path loss. d is the direct distance in the 3D space. f_c is the center frequency in MHz. A_B is the attenuation of the building, which we set to 40 dB as in [29]. The received power P_{rx} [dB] is determined as

$$P_{rx} = P_{tx} - PL + G_t + G_r, \tag{15}$$

where P_{tx} [dB] is the transmitted power. G_t [dB] is the airBS antenna gain that could be of a directional antenna. G_r [dB] is the gUT antenna gain.

Finally, the SINR for the signal received from the i-th airBS is calculated similarly to the study [43]

$$SINR_i = \frac{P_{rx,i}}{\sum I_{/i} + N} \tag{16}$$

where $P_{rx,i}$ [dB] is the received power from the i-th airBS, $I_{/i}$ is the interference from all airBSs except the i-th airBS and N [dB] is the noise.

Therefore, the service time $\mathcal{T}$ is the average time the j-th gUT spends in LoS and in connection with the i-th airBS. This is the time between handovers and we will determine it empirically from the ray-tracing simulation in Section IV.

III. SIMULATION

This section details our developed game engine-based synthetic 3D urban layout generator, as well as the setup for the ray-tracing simulation.

A. 3D URBAN LAYOUT GENERATOR

We conduct our experiments using the Python programming language. We use the game engine **Panda3D** to generate the 3D urban environment, including buildings, gUTs, airBS, and mobility manager, to calculate the movement trajectories of different components. The building positions are distributed grid-like, with a density of $\alpha\beta$ per square kilometer. The widths of buildings and streets are calculated based on (3) and (4).

The mobility manager is implemented using PandAI, which is an artificially intelligent (AI) engine that is included in Panda3d. It can manage different types of mobility patterns, including human mobility, pathfinding, and group mobility. To provide human-like mobility, we generate a navigation mesh with grid positions spaced evenly, with a step size equal to $w_b + w_s$. The mobility manager randomly selects the mobility targets for gUT and airBS from the navigation mesh nodes. Then, the AI engine uses the navigation mesh to determine the shortest path to set the mobility trajectory using the star algorithm.

Panda3D not only simplifies the implementation of a large synthetic 3D urban environment, but it also provides a straightforward method for retrieving and calculating transformations and relative transformations. This method is particularly useful for determining directional antenna transformations and ray-tracing. Using custom Panda3D tasks, we periodically collect the transformations and ray-tracing LoS condition metrics every second.

This article uses the term "actor" in game engines to describe mobile elements with the ability to move, like gUTs and airBSs. The ground users represent a human-like actor

who has a gUT node attached to his right hand. The airBSs are represented by quadcopters. Each quadcopter has a total volume of one cubic meter.

B. SIMULATION SETUP

As we previously outlined the implementation method for urban layouts and the network elements, this section delves into the simulation setup and parameters. We conducted several experiments on the standard urban layouts, which are suburban, urban, dense urban, and high-rise urban.

In addition, urban environment is generated using PPP distribution by iterating over the three ITU-R parameters (α, β, γ) to generate 64 urban layouts by linearly spacing the α parameter from 0.1 to 0.7, the β parameter from 750 to 100 buildings in a square kilometer, and γ from 8 to 50 meters. We divide each range into 4 segments. We then combine the segments to generate 64 urban layouts. To ensure the scalability of the proposed model, we add the standard layout and some selected layouts from previous work. As a result, we simulated 90 urban layouts in total. Figure 4 shows the resultant random distribution of urban environments.

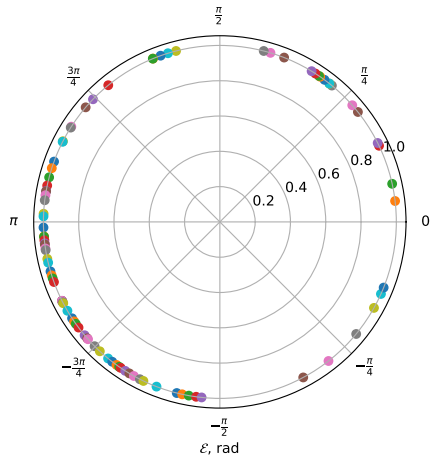

FIGURE 4. The resultant random distribution for urban environments

In each urban layout, we generate 10 human-like ground actors with 10 gUTs that are attached to the actors' hands and 10 quadcopter UAVs with 10 airBSs. We randomly distribute the ground actors by selecting their positions from the navigation mesh grid nodes. The height of the gUTs ranges from 1 to 1.5 meters, depending on the actor's hand movement during the walk. We randomly select the positions of airBSs from the navigation mesh nodes, while each airBS is located at a different height range from 50 to 1000 meters.

Moreover, the mobile ability is enabled for the gUTs and the airBS, where the velocity of the gUT is set to 3 [m/s] while the velocity of the airBS is set to 30 [m/s]. We randomly select the initial locations and the mobility target locations from the navigation mesh grid. The trajectories of the movement for gUTs and airBSs are calculated based on selecting the shortest path using the star algorithm, which is included within the PandaAI engine.

We calculate the radio link budget for the A2G communication channel at a center frequency of 28 [GHz]. We set the airBS's transmit power to 43 [dB] and the omnidirectional antenna's antenna gain to 1 [dB]. We calculate the directional antenna gain based on its radiation pattern. The signal's attenuation through a building is 40 [dB].

Finally, the simulation is run for 400 seconds while the ray-tracing LoS condition and the transformation of gUTs and airBSs are collected every second. The omnidirectional and the directional ray-tracing are collected in the same transformations. We conduct analysis and data visualization using NumPy, SciPy, and other Python libraries.

IV. RESULTS

This section discusses the results of our experiments and highlights the most important findings. First, we discuss dataset balancing and the impact of urban layouts on the LoS and NLoS classes. Next, we deeply and elaborately analyze the ray-tracing LoS for omnidirectional and directional scenarios to come up with the final bivariate joint probability function P_{LoS}. Then, we discuss the generality of our proposed P_{LoS} for the omnidirectional scenario and benchmark its performance for the directional scenario. Finally, we discuss the effect of mobility on connection time and introduce two service time models for the omnidirectional and directional scenarios.

A. DATA BALANCING

Despite the clean and organized nature of the collected data from the ray-tracing simulation, we observe an imbalance between the positive LoS and negative NLoS classes, regardless of the distribution of gUTs and airBSs. For example, suburban-like layouts have a high probability of having positive LoS because of their large street widths and lower building heights. Figure 5 depicts the percentage of positive LoS samples to the total samples along the environment layout range as represented using the complex argument of the layout. It shows that the LoS class is the majority class in most urban layouts of the omnidirectional scenario except in the range around $\mathcal{E} = -2$ radian, where the positive LoS is the minority class or almost near the middle of the figure. That means less P_{LoS} in the dense and high-rise urban layouts because of the narrow streets and high buildings.

When using directional antennas on airBSs, the majority class of the ray-tracing simulation is the negative NLoS. The second line plotted in Figure 5 shows the positive LoS of the directional scenarios. The positive LoS class's mean percentage is 75.22% for the omnidirectional scenario and 13.73% for the directional scenario. This imbalance toward the positive LoS in omnidirectional and the NLoS in directional scenarios could cause a bias in the modeling process and the model's performance.

To resolve this imbalance, we use the SMOTE [44] (the synthetic minority oversampling technique), which is an oversampling technique used in statistics and machine learning

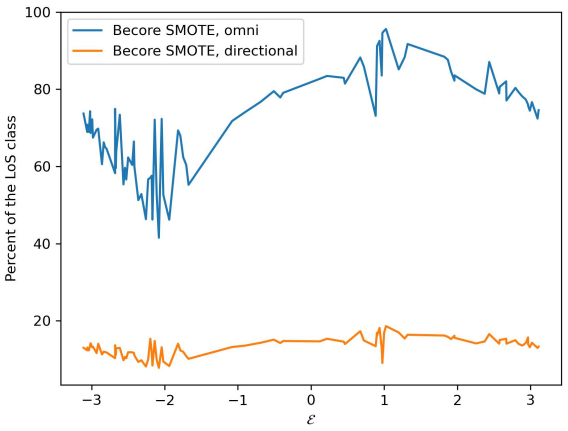

FIGURE 5. The percentage of the LoS class for omnidirectional and directional scenarios show imbalanced data, before using the SMOTE technique.

to address imbalanced datasets. To balance the class distribution, it specifically generates synthetic samples from the minority class. In our case, the NLoS in the omnidirectional scenario and the LoS class in the directional scenario represent the minority class. The SMOTE application changes the size of the collected ray-tracing datasets. For example, the average number of records before the SMOTE is 41,751 for both omnidirectional and directional scenarios. The average number of records after the SMOTE is 51,650 for the omnidirectional scenario and 57,158 for the directional scenario, respectively. Before the SMOTE, the total number of records in the dataset was 3,775,022, and after the SMOTE, it was 4,550,590. The SMOTE balanced the LoS and NLoS to 50% for each. For more details about oversampling and the SMOTE, refer to [44].

B. RAY-TRACING ANALYSIS

We use numerical methods to turn the column-like ray-tracing dataset into a 2D histogram and a 2D smoothed surface matrix for both omnidirectional and directional cases to find the joint PDF, CDF, and marginal functions. After we formulate our model P_{LoS} as a joint CDF function, we provide the surface fitting parameters of the proposed model as polynomial functions of the urban complex argument.

1) Omnidirectional Scenario

To determine the approximate joint PDF $f(x, y)$, we analyze the 2D histogram of the vector (X, Y) for the four standard urban layouts. The 2D histogram densities are shown in Figures 6 to Figure 9 for high-rise urban, dense urban, urban, and suburban, respectively. We calculate the 2D histogram using the positive ray-tracing LoS condition with (40×40) bins. From the four figures, one can see a similar distribution to the normal or normal-like in the direction of y (the altitude difference between transmitters and receivers), while the distribution in the x direction (ground distance direction) is affected by urban layouts, while the figures show different density distributions. For several reasons, we can't see a pattern that looks like a known distribution along the x-axis. These include (1) the small sample size compared to the wide range of the random variables; (2) the street canyons give a positive LoS condition at long ground distances no matter what y is; and (3) situations with high γ, like those shown in Figures 6 and 7, which have lower density near the zero of the x-axis because of the heights of the buildings.

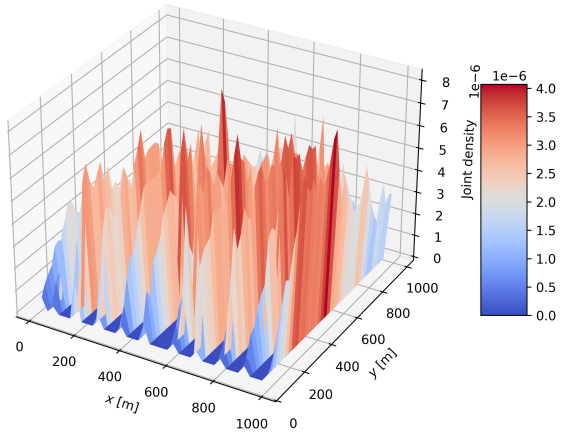

FIGURE 6. High-rise urban, 2D histogram density distribution of (X, Y) for positive ray-tracing LoS.

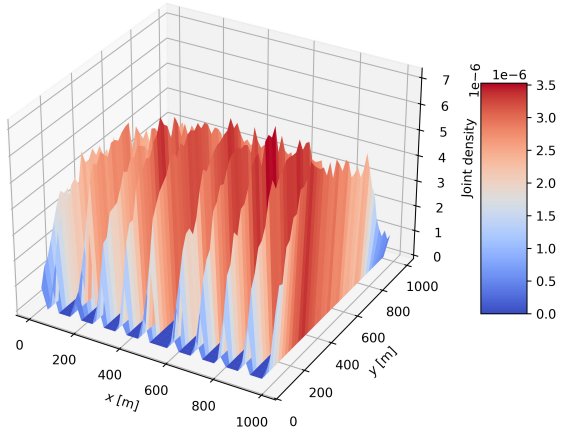

FIGURE 7. Dense urban, 2D histogram density distribution of (X, Y) for positive ray-tracing LoS.

Additionally, Figures 6 to 9 are examples of representing the ray-tracing probability distribution in a 2D matrix that is equivalent to $f(x, y)$. To distinguish the numerical matrix from the theoretical model, we denote the numerical one by $f_m(x, y)$. To validate the $f_m(x, y)$ matrix, we use the cumulative sum to ensure that $\sum f_m(x, y) \approx 1$ as expressed in (8), which we find valid. Although $f_m(x, y)$ is a well-constructed joint

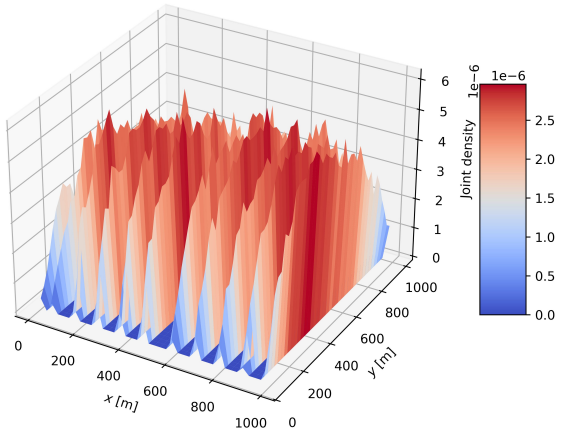

FIGURE 8. Urban, 2D histogram density distribution of (X, Y) for positive ray-tracing LoS.

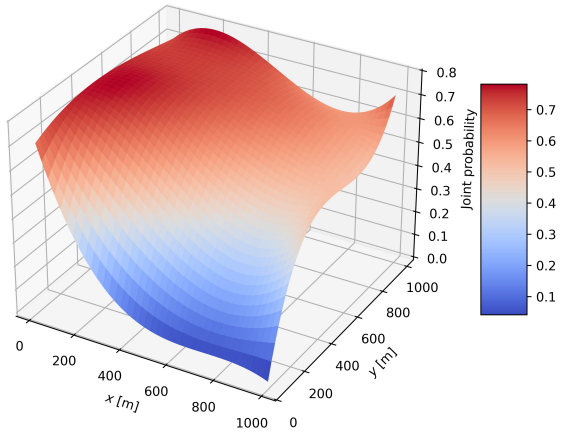

FIGURE 10. High-rise urban, 2D joint probability of (X, Y) for positive ray-tracing LoS.

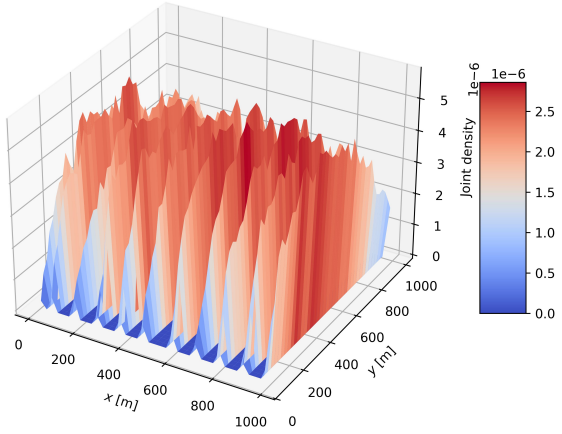

FIGURE 9. Suburban, 2D histogram density distribution of (X, Y) for positive ray-tracing LoS.

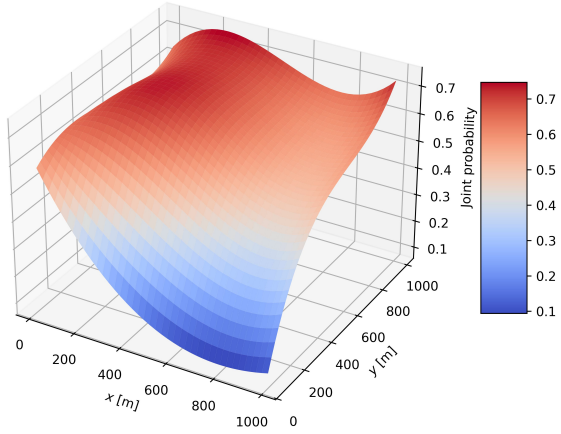

FIGURE 11. Dense urban, 2D joint probability of (X, Y) for positive ray-tracing LoS.

probability, it cannot reveal the marginal functions because of the independent nature of the X and Y random variables, which implies mutual scaling according to (11) and (12).

Moreover, we can see in Figures 6 to 9, that the distribution in the Y direction is dominant and makes it challenging to infer the marginal function of the X random variable from the joint density distribution matrix. To solve this problem, we approximate the probability in (10) from the positive ray-tracing LoS by calculating the mean probability at every vector (X, Y). This allows us to construct a 2D joint matrix that represents the CDF, as in (13). We denote the estimated 2D joint matrix as $F_m(x, y)$. Because the estimated $F_m(x, y)$ is quite jumpy, we fit its surface using a bivariate cubic spline. The results of the bivariate cubic spline fitting are shown in Figures 10 to 13.

The Figures 10 to 13 confirm the findings from the 2D histogram density. It shows a similar curve to the error function in the y-axis, which is highly probable to be the CDF of one of the normal-like distributions. The concavity of the surface in the range 600 to 1000 along the x-axis near the upper limit of the y-axis in the four sub-figures is related to the nature of the bivariate cubic spline used in the surface fitting and the existence of few positive LoS at a far distance and high altitude especially when the LoS ray is along a street's canyon. From Figure 10 to Figure 13, the most important thing to notice is that the marginal functions in (11) and (12) can be written as an exponential and a normal-like CDF, respectively. This finding agrees with [28], which found that the LoS is exponentially distributed as a function of ground distance (x).

Moreover, we use numerical estimation to find the curves of the marginal functions (17) and (18) to make sure that the joint probability function is made up of two marginal functions that can be shown by an exponential function and a

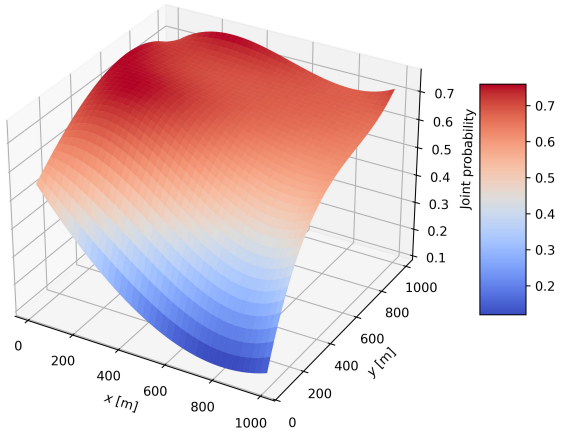

FIGURE 12. Urban, 2D joint probability of (X, Y) for positive ray-tracing LoS.

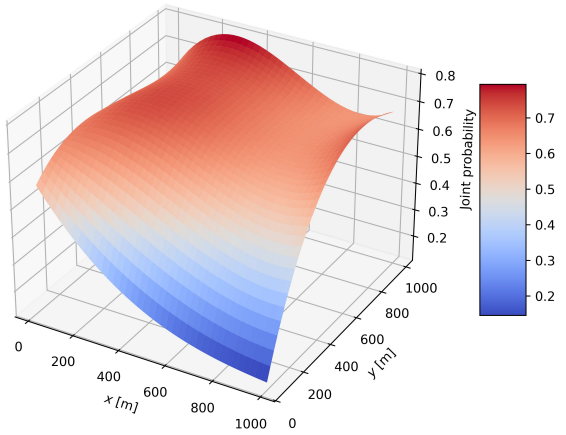

FIGURE 13. Suburban, 2D joint probability of (X, Y) for positive ray-tracing LoS.

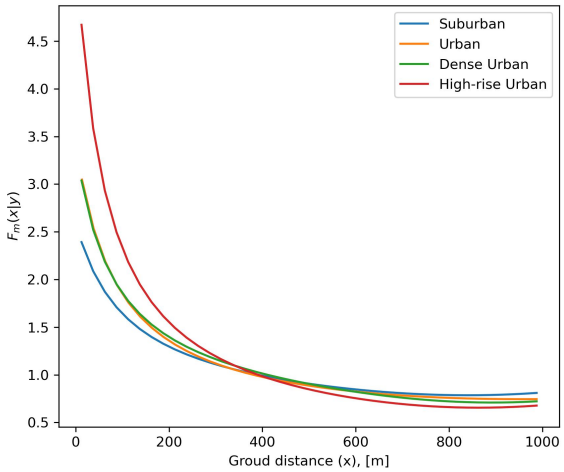

FIGURE 14. Marginal function $F(x|y)$ for the four standard urban layouts and positive ray-tracing LoS using omnidirectional antennas on the airBSs.

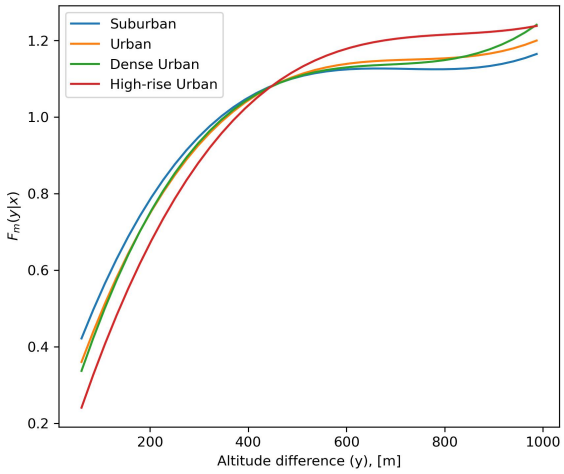

FIGURE 15. Marginal function $F(y|x)$ for the four standard urban layouts and positive ray-tracing LoS using omnidirectional antennas on the airBSs.

CDF of a normal distribution. The conditional marginal CDF function in the x direction is denoted by $F(x|y)$ and calculated by (17).

$$F(x|y) \approx F_m(x|y) = \frac{F_m(x,y)}{F_Y(y)}, \tag{17}$$

where $F_Y(y) = \sum F_m(x,y)$ in the y direction. Similarly, $F(y|x)$ is the conditional marginal CDF function in the y direction and is given by (18)

$$F(y|x) \approx F_m(y|x) = \frac{F_m(x,y)}{F_X(x)}, \tag{18}$$

where $F_X(x) = \sum F_m(x,y)$ in the x direction. If you want to find the numerical value of the marginal functions $F_X(x)$ and $F_Y(y)$, you just add up the joint matrix in the same direction as the variable, as explained in [45]. Figures 14 and 15 show that the conditional marginal functions are scaling one another, which agrees with the theoretical definition in [45].

Now, we can reformulate the joint bivariate LoS probability function in (13) as a product of the exponential and the CDF of the normal distribution as expressed in (19)

$$P_{LoS}(x,y) = \frac{1}{2}\exp\left(-\frac{a\alpha x}{\sqrt{2}\pi\beta}\right)\left(1 + erf\left[\frac{by}{w_s\sigma}\right]\right), \tag{19}$$

where $\sigma = (2 - \pi/2)\gamma$ is the standard deviation of the Rayleigh distribution while a and b are the surface fitting parameters. The term $\frac{\alpha}{\sqrt{2}\pi\beta}$ is used to scale the variable x to reduce the variance of a. Similarly, the term $\frac{1}{w_s\sigma}$ is used to scale the variable y to reduce the variance of b.

Because it is possible to conceal the scale part of the log-normal within the exponential function, we simplify (19) into

(20)

$$P_{LoS}(x,y) = exp\left(-\frac{a\alpha x}{\sqrt{2}\pi\beta}\right) erf\left(\frac{by}{w_s\sigma}\right), \quad (20)$$

The joint PDF function can be determined by the second partial derivative of (20). The derivative is solved using an online mathematical tool called WolframAlpha [1] as expressed in (21).

$$f(x,y) = -\frac{\sqrt{2}ab\alpha}{\pi^{1.5}\beta w_s\sigma} exp\left(-\frac{a\alpha x}{\sqrt{2}\pi\beta}\right) erf\left(\frac{by}{w_s\sigma}\right). \quad (21)$$

2) Directional Scenario

We collect the ray-tracing LoS for both omnidirectional and directional scenarios, as previously mentioned. In directional scenarios, we collect the ray-tracing LoS whenever the ray connecting gUT and airBS satisfies two conditions. First, there is a positive ray-tracing LoS. Second, the elevation and azimuth angles of the direct ray connecting the airBS and gUT are located within the main lobe of the directional antenna. Let's denote the omnidirectional ray-tracing LoS condition by $P_{TR,o}$, the directional ray-tracing LoS by $P_{TR,d}$, and the elevation and azimuth angles of the ray connected between the airBS and the gUT are denoted by θ and ϕ, respectively. The $P_{TR,d}$ can be positive if the ray angles θ and ϕ are located within the main lobe of the directional antenna, and the $P_{TR,o}$ is also positive LoS. We mathematically express these two conditions in (22).

$$P_{TR,d} = \begin{cases} P_{TR,o}, & if \frac{-\theta_{3dB}}{2} \leq \theta \leq \frac{\theta_{3dB}}{2}, \frac{-\phi_{3dB}}{2} \leq \phi \leq \frac{\phi_{3dB}}{2}, \\ 0, & otherwise. \end{cases} \quad (22)$$

In other words, the simulation simultaneously collects the directional and omnidirectional data of the ray-tracing LoS. The provided dataset records the $P_{TR,d}$ and $P_{TR,o}$ fields with the relative transformation of the gUT to the LCS of the airBS. This method of collecting the ray-tracing ensures that the SMOTE balancing technique receives the same input variables in both omnidirectional and directional scenarios.

The results of this method show that the directional ray-tracing has similar joint probability and similar marginal functions to those we find in the omnidirectional scenario. The joint probability and the marginal function have the same trends; however, scale-down values are shown in Figures 16, 17, and 18. Figure 16 shows an example of the joint probability for the high-rise urban layout. Figure 17 shows the conditional marginal function in the x direction, while Figure 18 shows the conditional marginal function in the y direction. All three figures are similar to those we present in the omnidirectional scenario but with lower values.

3) The Surface Fitting

From the previous results, we can decide that the model in (20) can be used to predict the LoS probability for both omnidirectional and directional scenarios. For the proposed unified model in (20), we use the surface fitting method to come up with the fitting parameters, a and b, which depend on the complex argument of the urban layout. The surface fitting results produce four formulas. The functions $a_o(\mathcal{E})$ and $b_o(\mathcal{E})$ calculate parameters a and b for the omnidirectional scenario, respectively. For the directional scenario, the functions $a_d(\mathcal{E})$ and $b_d(\mathcal{E})$ provide a and b, respectively.

For the omnidirectional scenario, the fitting parameters of the unified proposed model in (20) are given in (23) and (24).

$$a_o(\mathcal{E}) = 0.16\mathcal{E}^3 - 0.87\mathcal{E}^2 - 1.20\mathcal{E} + 8.63 \quad (23)$$

$$b_o(\mathcal{E}) = -0.001\mathcal{E}^3 - 0.11\mathcal{E}^2 - 0.01\mathcal{E} + 1.31 \quad (24)$$

[1] WolframAlpha is available online at https://www.wolframalpha.com/

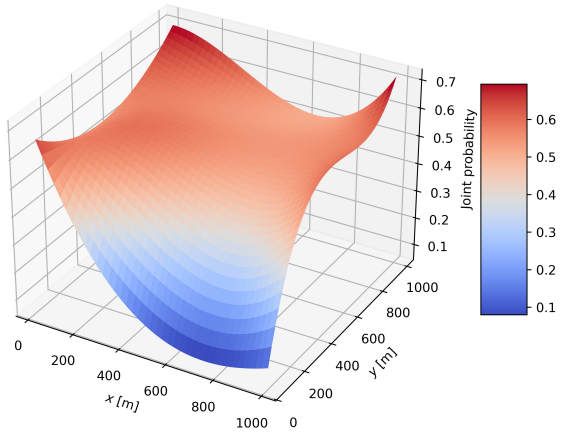

FIGURE 16. High-rise urban, 2D joint probability of (X, Y) for positive ray-tracing LoS using directional antennas on the airBSs.

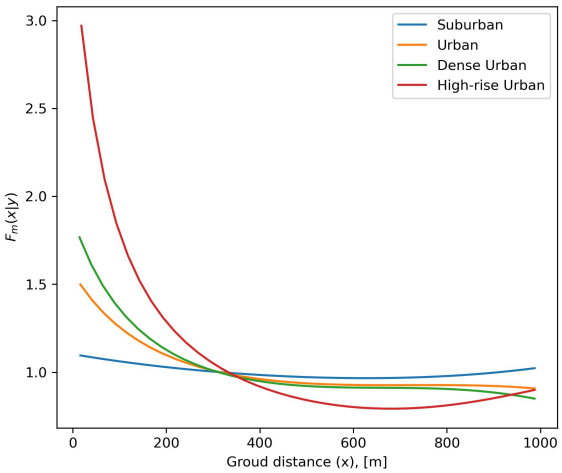

FIGURE 17. Marginal function $F(x|y)$ for the four standard urban layouts for positive ray-tracing LoS using directional antennas on the airBSs.

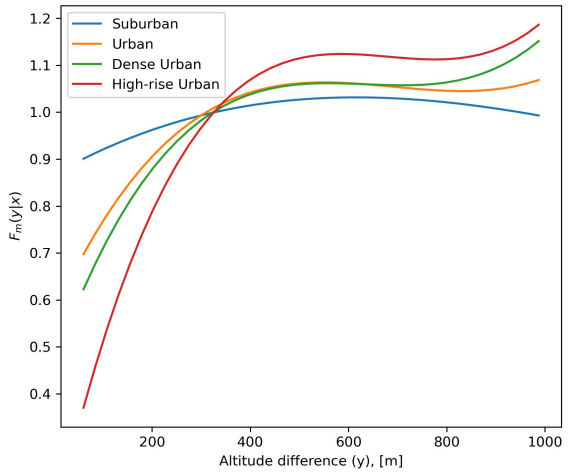

FIGURE 18. Marginal function $F(y|x)$ for the four standard urban layouts for positive ray-tracing LoS using directional antennas on the airBSs.

For the directional scenario, the fitting parameters of the unified proposed model in (20) are given in (25) and (26).

$$a_d(\mathcal{E}) = 0.02\mathcal{E}^3 - 0.60\mathcal{E}^2 - 0.15\mathcal{E} + 6.45 \quad (25)$$

$$b_d(\mathcal{E}) = -0.008\mathcal{E}^3 - 0.072\mathcal{E}^2 + 0.06\mathcal{E} + 0.96 \quad (26)$$

The surface fitting parameters are depicted in Figure 19 as functions of urban layout complex argument $\mathcal{E}$.

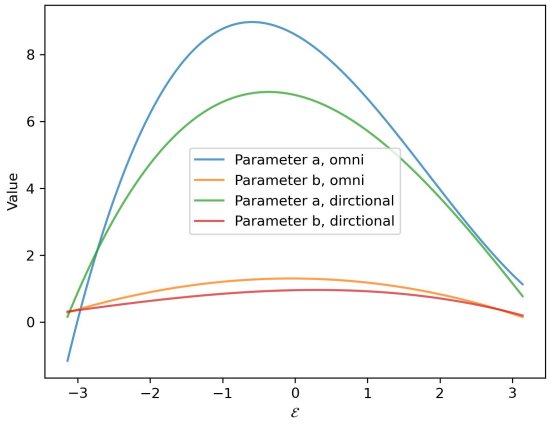

FIGURE 19. Fitting parameters for both omnidirectional and directional scenarios.

C. GENERALITY OF THE PROPOSED MODEL

In the previous section, we formulate the proposed unified P_{LoS}. In this section, we are going to validate our proposed models against the ray-tracing collected data and discuss their generality by comparing their performance to a few recent models. We compare our proposed model to the latest models in the art. The models we compared with are [16], [17], [28], [29]. Although the model [16] is not new, we include it in the comparison because it uses the exponential function and the error function, both of which are used in our model. Similarly, the model [17] uses the exponential function and the log-normal CDF. The generality analysis is discussed for the performance of the omnidirectional scenario, while the performance of the directional scenario is introduced as a benchmark.

TABLE 4. Confusion matrix

	Predicted	
	LoS	NLoS
Actual ray-tracing LoS	TP	FN
Actual ray-tracing NLoS	FP	TN

1) Omnidirectional Scenario

To demonstrate the generality of the proposed model, we generated a large number of synthetic urban layouts, as illustrated in Section III, that describe the simulation setup. We use a relatively larger simulation area than those used in previous works. For example, in [29], a simulation area equal to $(w_s+w_b)^2 - w_b^2$ is used, whereas we use 1.2 square kilometer. Another difference is the range of the airBS altitude; we use a range from 50 to 1000 meters, while previous works used selected heights, such as 100, 300, and 500 meters.

To validate the generality of the proposed model, we use root mean squared error (RMSE), accuracy, precision, and recall. We avoid using the R-squared metrics because we find their small range, between 0 and 1, unsuitable for the LoS probability, which has the same small range. The jumpy nature of the ray-tracing LoS is another reason for not using R-squared because it produces a variance that is larger than one in large joint matrices.

Figure 20 depicts the RMSE metric. The proposed model scores the lowest RMSE overall in the range $[-\pi, \pi]$ that represents the complex argument of urban layouts. For more information on how to represent an urban layout using a complex argument, see Section II-A.

For mm-wave and terahertz signals, the binary representation of the LoS probability makes more sense because of the large attenuation of the signal caused by blockage. Therefore, we round the results of the tested models to produce a binary representation of the LoS probability as LoS and NLoS classes. The confusion matrix is commonly used to describe and evaluate binary classification models.

The confusion matrix [44], as expressed in Table 4, shows four states of comparison between a model's prediction result and the actual ray-tracing LoS condition. The four states are, namely, true positive (*TP*), false negative (*FN*), false positive (*FP*), and true negative (*TN*). The *TP* is the number of having the ray-trace LoS, while the prediction of the tested model is LoS, too. The *FN* is the number of having LoS from the ray-tracing, but the prediction of the tested model is NLoS. Similarly, the *FP* counts the ray-tracing NLoS and the predicted LoS, while the *TP* counts the ray-tracing NLoS

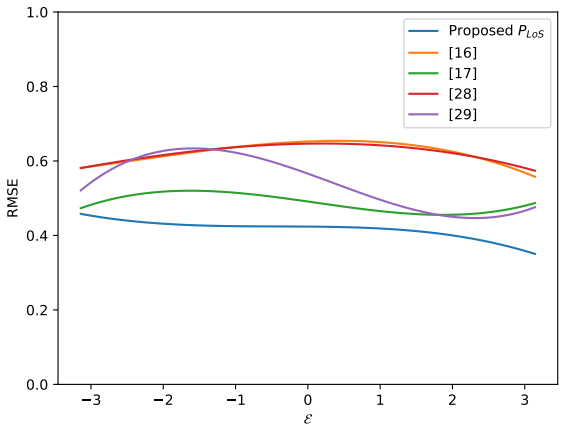

FIGURE 20. The root mean square error (RMSE) between the models' predictions and $F_m(x, y)$ spans the entire complex argument of urban layouts.

if the prediction is also NLoS.

The accuracy metric is defined as the ratio of correct predictions to the total number of predictions. The accuracy is expressed in (27).

$$Accuracy = \frac{TP + TN}{TP + FN + FP + TN}. \tag{27}$$

Figure 21 depicts a comparison of the average accuracy models. It shows that our proposed model outperforms previous models in most of the complex argument $\mathcal{E}$ range.

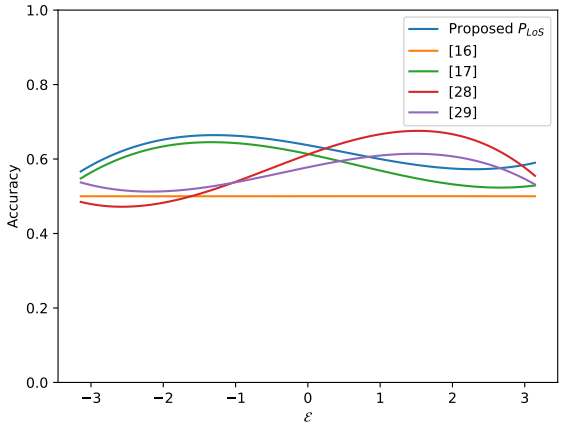

FIGURE 21. The accuracy of the models' predictions spans the entire complex argument of urban layouts.

To analyze the precision of the models, we use (28). Figure 22 shows that the average precision of the proposed model is better with a small difference than the model [29], while [17] has good precision on dense and high-rise urban layouts but does not perform well in suburban and urban layouts. [28] is useful in suburban layouts.

$$Precision = \frac{TP}{TP + FP}. \tag{28}$$

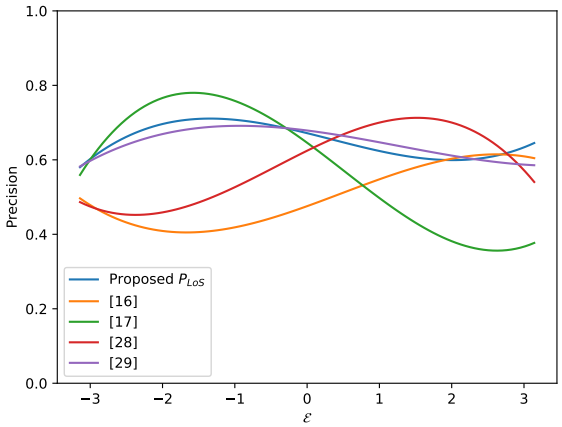

FIGURE 22. The precision of the models' predictions span the entire complex argument of urban layouts.

The recall performance metric measures the LoS predicted class to the total actual LoS and is expressed as in (29), The recall is also known as the sensitivity.

$$Recall = Sensitivity = \frac{TP}{TP + FN}. \tag{29}$$

Figure 23 shows the average recall for both predicted LoS and NLoS. In this metric, the proposed model outperforms the previous models, followed by the model [17]. The order of models in Figure 22 and Figure 23 indicates a kind of instability in the prediction of previous models, which we will analyze in the next paragraph.

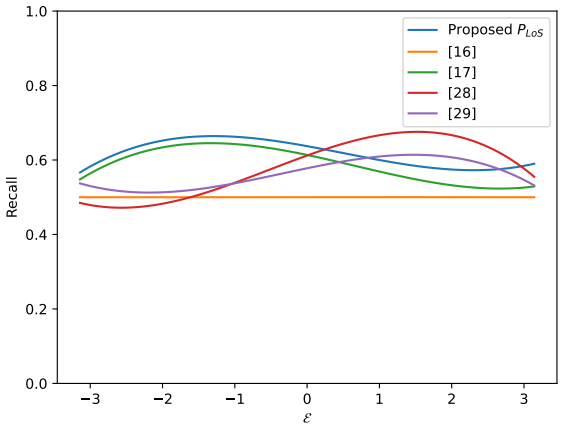

FIGURE 23. The recall (sensitivity) of the models' predictions spans the entire complex argument of urban layouts.

We analyze the possible bias of the model's prediction by focusing on the positive LoS class. Figure 24 shows the results of analyzing only the positive predicted LoS class to the actual ray-tracing positive class. It shows that the model [17] has high sensitivity to LoS class, and the opposite can be said

about [29]. The model [28] depends on the urban environment, where it has a sensitivity to LoS class in suburban-like environments. However, the exponential term in [16] seems to be dominant, with near zero sensitivity to the positive LoS class. The proposed model has balanced predictions for both LoS and NLoS, and its results in Figure 24 show a similar pattern and level as those in Figure 21, Figure 22, and Figure 23.

To quantify the bias of models, we calculate it as a percentage of the average recall of the LoS class to the weighted average recall. The model [16] has almost 100% bias to the NLoS class, while [17] has about 67% bias to the LoS class. The model [29] has about 53% bias to the NLoS class. The model [28] has a bias to both classes depending on the urban layout. In dense and high-rise urban layouts, it exhibits 56% bias towards the NLoS, whereas in suburban and urban layouts, it exhibits 55% bias towards the LoS class. The proposed model shows a small bias toward the LoS at the beginning of the $\mathcal{E}$ range, while the average bias over the range is less than one percent toward the LoS class.

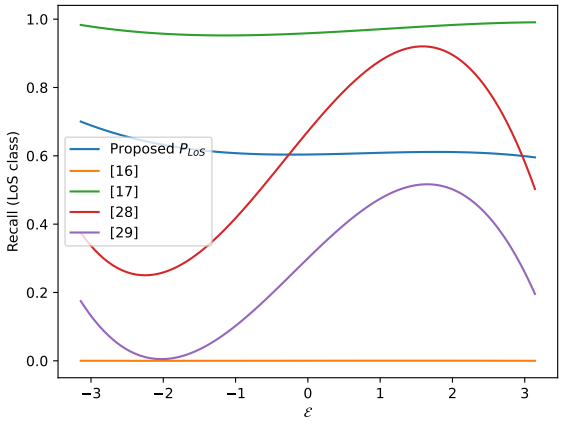

FIGURE 24. The recall (sensitivity) of the prediction of models as analyzed for positive LoS class.

Moreover, we have tested some specific scenarios, such as the tested environments in [29]. For example, we generate a synthetic layout for Cologne City, Germany, using ($\alpha = 0.55, \beta = 680, \gamma = 12.69$) over an area of 1200 square meters. We find that our proposed model outperforms the previous model, whose RMSE was 0.42, while 0.45 and 0.52 were scored for [17] and [29], respectively. Table 5 lists the overall weighted average of the analyzed performance metric. The recall has almost identical values to the accuracy because of the effect of balancing the dataset; thus, Figure 24 provides a better visualization of this metric. The F1-score is calculated from the precision and the recall as expressed in (30).

$$F_1 = 2\frac{precision \cdot recall}{precision + recall}. \tag{30}$$

TABLE 5. Weighted average of the presented metrics for the overall range of urban layout complex argument.

Metric	[16]	[17]	[28]	[29]	The proposed P_{LoS}
RMSE	0.62	0.49	0.62	0.54	0.41
Accuracy	0.50	0.58	0.58	0.56	0.62
Precision	0.49	0.58	0.58	0.64	0.65
Recall	0.50	0.58	0.58	0.56	0.62
F1-score	0.33	0.50	0.55	0.48	0.58

2) Benchmark the Directional Scenario

To the best of our knowledge, our proposed unified model is the first effort modeling the P_{LoS} for the directional antenna scenario, so we benchmark its performance for the directional scenario as shown in Figure 25. The averages of the analyzed metrics for the whole 90 urban layouts are 0.32, 0.53, 0.55, 0.53, and 0.61 for RMSE, accuracy, precision, recall, and class LoS recall, respectively. The proposed unified model (20) works about the same in both directional and omnidirectional situations, with accuracy and recall values that are very close to each other. In the directional scenario, the proposed model shows about 15% bias to the positive LoS class, whereas in the omnidirectional scenario, it has less than 1%.

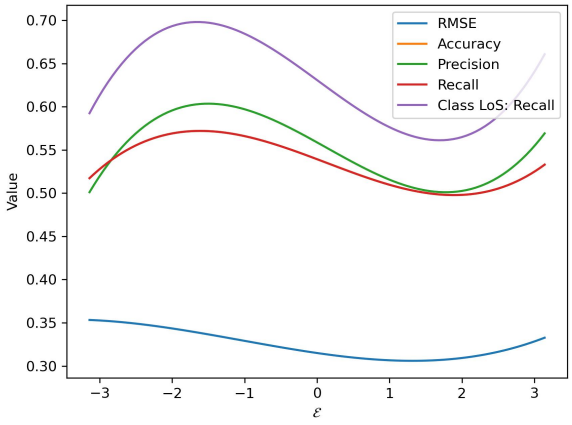

FIGURE 25. The RMSE, accuracy, precision, recall of the proposed model's predictions spans the entire complex argument of urban layouts.

D. THE SERVICE TIME

In previous results, we demonstrate the generality of our unified proposed model and benchmarked its performance in the directional scenario. In this section, we present another benchmark of the service time (sojourn time). Using the optimal SINR connection, we calculate the service time by averaging the intervals between handovers. Ten gUTs and two airBSs are used. To analyze the impact of the airBS height on the service time, we simulate the airBSs at 100, 300, and 500 meters. The gUTs and the airBSs are moving according to the mobility model in Section II-C. The connection is established according to the best SINR it gets from airBSs based on the

ray-tracing LoS and the models in Section II-E. We run the simulation for a total of 120 seconds for each urban layout. A total of 67 urban layouts are simulated, as described in Section III-B.

For the omnidirectional scenario, we find that the suburban and urban-like layouts have the maximum service time. The maximum measured time between handovers was 87 seconds for airBS heights of 300 and 500 meters. At 100 meters high, the maximum measured time between handovers was 60 seconds. In the directional scenario, the maximum measured time between handovers was about 37 seconds for altitudes of 100 meters, while it was 31 seconds for 300 and 500 meters. Figure 26 shows the average service time for omnidirectional and directional scenarios as a function of the urban layout complex argument.

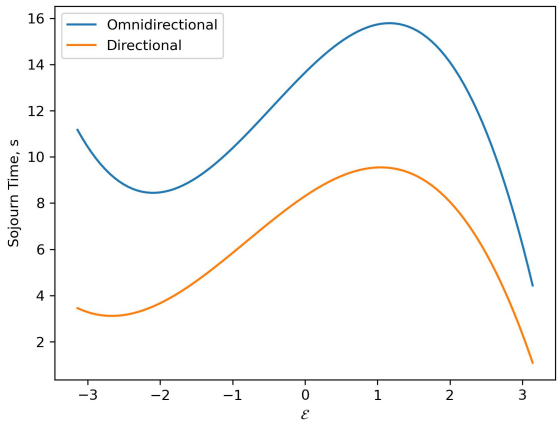

FIGURE 26. The average service time for omnidirectional and directional scenarios.

As shown in (31) and (32), the service time is modeled as a cubic polynomial function of the urban layout's complex argument. The service time for the omnidirectional scenario is $\mathcal{T}_o$, and for the directional scenario is $\mathcal{T}_d$. The expressions in (31) and (32) represent the findings where the airBS altitude is 300 and 500 meters. The average service time was 11.66 seconds for the omnidirectional scenario and 6.26 seconds for the directional scenario. For an altitude of 100 meters, we get the same pattern with almost the same average service time in the omnidirectional scenario, while the average time in the directional scenario is 7.2 seconds.

$$\mathcal{T}_o = -0.42\mathcal{E}^3 - 0.59\mathcal{E}^2 + 3.09\mathcal{E} + 13.65 \quad (31)$$

$$\mathcal{T}_d = -0.25\mathcal{E}^3 - 0.61\mathcal{E}^2 + 2.09\mathcal{E} + 8.31 \quad (32)$$

In the directional scenario, we find that using a directional antenna on the airBS has improved the average SINR from 19.54 dB in the omnidirectional scenario to 26.90 dB in the directional scenario, by an average increase equal to 38%. The average throughput per user increased by 43% from 467.6 Mbps in omnidirectional to 670 Mbps in directional. The spectral efficiency is enhanced by 43% from 46.76% to 67%. However, the service time dropped by 46% from 11.66 seconds to 6.26 seconds.

V. LIMITATIONS

This section highlights some important limitations of the proposed ray-tracing simulation method. First, we notice that the Panda3D calculates spherical boundaries of objects, which makes it challenging to find a trajectory for gUT mobility in urban layouts of narrow streets. To produce human-like mobility, the gUTs need to avoid colliding with buildings, while the spherical boundaries of buildings act as blockers of movement. To solve this problem, we reduced the range of α to between 0.1 and 0.7 instead of 0.1 to 0.8. Future work can test another solution by trying tight boundaries.

We find that the first fitting of the a and b parameters has an average RMSE of about 0.12, which is better than the reported results. To provide a and b parameters as a function of urban layout complex argument as in (23), (24), (25), and (26) is important to generalize the model in the ITU-R context. However, it is a challenging task to fit the coefficients of equations in (23), (24), (25), and (26) because of the need to simulate a large number of urban layouts. We find that simulating 67 urban layouts provides better performance than the existing model and ensured that increasing the number of layouts to 90 enhanced the performance. As a result, we share our source code on GitHub [42] for future research that requires ray-tracing simulation in synthetic urban environments.

VI. CONCLUSION

The LoS probability model is an essential part of the communication between gUTs and airBSs. Current literature lacks models that are built for the scenario where airBS is equipped with a 3GPP directional antenna. Furthermore, the impact of mobility on the state of LoS remains largely unexplored. These aspects are crucial for planning MEC-assisted wireless networks, so this study focuses on the mobility-aware aspects of the LoS probability model. In this study, we develop a game engine-based synthetic urban layout generator to simulate ray-tracing between airBSs and gUTs. Then, we propose a unified bivariate P_{LoS} model that could predict the LoS probability for both omnidirectional and directional scenarios for any ITU-R P.1410-5 urban layout. We validate the proposed P_{LoS} model by simulating ray-tracing on 90 synthetic urban layouts. We validated our proposed model, and the results show that it outperforms previous modes designed for an omnidirectional scenario. In the directional scenario, we provide a benchmark for its performance. We also analyze the mobility impact on the LoS and proposed two models that estimate the service time for omnidirectional and directional scenarios. This research not only considers mobility-aware aspects but also provides environment-dependent modeling and a simple representation of the ITU-R P.1410 environment parameters, which opens new research directions to study the joint effect of mobility and environment on LoS probability, channel modeling, and MEC services.

REFERENCES

[1] Y. Han, H. Liu, Y. Wang, and C. Liu, "A Comprehensive Review for Typical Applications Based Upon Unmanned Aerial Vehicle Platform," *IEEE Journal of Selected Topics in Applied Earth Observations and Remote Sensing*, vol. 15, pp. 9654–9666, 2022.

[2] N. Cheng, S. Wu, X. Wang, Z. Yin, C. Li, W. Chen, and F. Chen, "AI for UAV-Assisted IoT Applications: A Comprehensive Review," *IEEE Internet of Things Journal*, vol. 10, no. 16, pp. 14 438–14 461, aug 2023.

[3] A. A. Khuwaja, Y. Chen, N. Zhao, M.-S. Alouini, and P. Dobbins, "A Survey of Channel Modeling for UAV Communications," *IEEE Communications Surveys Tutorials*, vol. 20, no. 4, pp. 2804–2821, 2018.

[4] ITU-R, "Propagation Data and Prediction Methods Required for the Design of Terrestrial Broadband Radio Access Systems in a Frequency Range from 3 to 60 GHz," Tech. Rep., 2012. [Online]. Available: https://www.itu.int/dms_pubrec/itu-r/rec/p/R-REC-P.1410-5-201202-I!!PDF-E.pdf

[5] ITU-R M.2135, "Guidelines for evaluation of radio interface technologies for IMT-Advanced," Tech. Rep., 2009.

[6] P. Kyösti, J. Meinilä, T. Jämsä, and L. Hentilä, "IST-4-027756 WINNER II D1. 1.2 V1. 2 WINNER II Channel Models," Tech. Rep. 82, 2007.

[7] 3GPP TR 38.900 - V14.2.0, "Study on channel model for frequency spectrum above 6 GHz," Tech. Rep., 2017. [Online]. Available: https://portal.etsi.org/TB/ETSIDeliverableStatus.aspx

[8] T. Bai, R. Vaze, and R. W. Heath, "Analysis of Blockage Effects on Urban Cellular Networks," *IEEE Transactions on Wireless Communications*, vol. 13, no. 9, pp. 5070–5083, 2014.

[9] M. K. Samimi, T. S. Rappaport, and G. R. MacCartney, "Probabilistic Omnidirectional Path Loss Models for Millimeter-Wave Outdoor Communications," *IEEE Wireless Communications Letters*, vol. 4, no. 4, pp. 357–360, aug 2015.

[10] I. Atzeni, J. Arnau, and M. Kountouris, "Downlink Cellular Network Analysis With LOS/NLOS Propagation and Elevated Base Stations," *IEEE Transactions on Wireless Communications*, vol. 17, no. 1, pp. 142–156, jan 2018.

[11] X. Liu, J. Xu, and H. Tang, "Analysis of Frequency-Dependent Line-of-Sight Probability in 3-D Environment," *IEEE Communications Letters*, vol. 22, no. 8, pp. 1732–1735, aug 2018.

[12] Z. Cui, K. Guan, C. Briso-Rodríguez, B. Ai, and Z. Zhong, "Frequency-Dependent Line-of-Sight Probability Modeling in Built-Up Environments," *IEEE Internet of Things Journal*, vol. 7, no. 1, pp. 699–709, jan 2020.

[13] J. Holis and P. Pechac, "Elevation Dependent Shadowing Model for Mobile Communications via High Altitude Platforms in Built-Up Areas," *IEEE Transactions on Antennas and Propagation*, vol. 56, no. 4, pp. 1078–1084, apr 2008.

[14] A. Al-Hourani, S. Kandeepan, and S. Lardner, "Optimal LAP Altitude for Maximum Coverage," *IEEE Wireless Communications Letters*, vol. 3, no. 6, pp. 569–572, dec 2014.

[15] L. Zhou, Z. Yang, G. Zhao, S. Zhou, and C.-X. Wang, "Propagation Characteristics of Air-to-Air Channels in Urban Environments," in *2018 IEEE Global Communications Conference (GLOBECOM)*, dec 2018, pp. 1–6.

[16] H. Kang, J. Joung, J. Ahn, and J. Kang, "Secrecy-Aware Altitude Optimization for Quasi-Static UAV Base Station Without Eavesdropper Location Information," *IEEE Communications Letters*, vol. 23, no. 5, pp. 851–854, may 2019.

[17] A. Al-Hourani, "On the Probability of Line-of-Sight in Urban Environments," *IEEE Wireless Communications Letters*, vol. 9, no. 8, pp. 1178–1181, aug 2020.

[18] M. Gapeyenko, D. Moltchanov, S. Andreev, and R. W. Heath, "Line-of-Sight Probability for mmWave-Based UAV Communications in 3D Urban Grid Deployments," *IEEE Transactions on Wireless Communications*, vol. 20, no. 10, pp. 6566–6579, oct 2021.

[19] A. Al-Hourani and I. Guvenc, "On Modeling Satellite-to-Ground Path-Loss in Urban Environments," *IEEE Communications Letters*, vol. 25, no. 3, pp. 696–700, mar 2021.

[20] Y. Hmamouche, M. Benjillali, and S. Saoudi, "Fresnel Line-of-Sight Probability With Applications in Airborne Platform-Assisted Communications," *IEEE Transactions on Vehicular Technology*, vol. 71, no. 5, pp. 5060–5072, may 2022.

[21] Q. Zhu, F. Bai, M. Pang, J. Li, W. Zhong, X. Chen, and K. Mao, "Geometry-Based Stochastic Line-of-Sight Probability Model for A2G Channels Under Urban Scenarios," *IEEE Transactions on Antennas and Propagation*, vol. 70, no. 7, pp. 5784–5794, jul 2022.

[22] M. Pang, Q. Zhu, Z. Lin, F. Bai, Y. Tian, Z. Li, and X. Chen, "Machine learning based altitude-dependent empirical LoS probability model for air-to-ground communications," *Frontiers of Information Technology & Electronic Engineering*, vol. 23, no. 9, pp. 1378–1389, 2022. [Online]. Available: https://doi.org/10.1631/FITEE.2200041

[23] M. Song, Y. Huo, Z. Liang, X. Dong, and T. Lu, "Air-to-Ground Large-Scale Channel Characterization by Ray Tracing," *IEEE Access*, vol. 10, pp. 125 930–125 941, 2022.

[24] V. Begishev, D. Moltchanov, A. Gaidamaka, and K. Samouylov, "Closed-Form UAV LoS Blockage Probability in Mixed Ground- and Rooftop-Mounted Urban mmWave NR Deployments," *Sensors*, vol. 22, no. 3, 2022. [Online]. Available: https://www.mdpi.com/1424-8220/22/3/977

[25] M. Pang, Q. Zhu, C.-X. Wang, Z. Lin, J. Liu, C. Lv, and Z. Li, "Geometry-Based Stochastic Probability Models for the LoS and NLoS Paths of A2G Channels Under Urban Scenarios," *IEEE Internet of Things Journal*, vol. 10, no. 3, pp. 2360–2372, feb 2023.

[26] M. Song, Z. Liang, Y. Huo, and R. Liu, "Line-of-sight probability for UAV communications in 3D grid urban streets," *Electronics Letters*, vol. 59, no. 20, p. e12979, 2023. [Online]. Available: https://ietresearch.onlinelibrary.wiley.com/doi/abs/10.1049/ell2.12979

[27] Y. Zhao, F. Zhou, L. Feng, W. Li, and P. Yu, "MADRL-Based 3D Deployment and User Association of Cooperative mmWave Aerial Base Stations for Capacity Enhancement," *Chinese Journal of Electronics*, vol. 32, no. 2, pp. 283–294, mar 2023.

[28] I. Mohammed, S. Gopalam, I. B. Collings, and S. V. Hanly, "Closed Form Approximations for UAV Line-of-Sight Probability in Urban Environments," *IEEE Access*, vol. 11, pp. 40 162–40 174, 2023.

[29] A. Saboor, E. Vinogradov, Z. Cui, A. Al-Hourani, and S. Pollin, "A Geometry-Based Modelling Approach for the Line-of-Sight Probability in UAV Communications," *IEEE Open Journal of the Communications Society*, vol. 5, pp. 364–378, 2024.

[30] A. Al-Hourani, "Line-of-Sight Probability and Holding Distance in Non-Terrestrial Networks," *IEEE Communications Letters*, vol. 28, no. 3, pp. 622–626, mar 2024.

[31] M. Lecci, P. Testolina, M. Polese, M. Giordani, and M. Zorzi, "Accuracy Versus Complexity for mmWave Ray-Tracing: A Full Stack Perspective," *IEEE Transactions on Wireless Communications*, vol. 20, no. 12, pp. 7826–7841, dec 2021.

[32] N. Chukhno, O. Chukhno, D. Moltchanov, S. Pizzi, A. Gaydamaka, A. Samuylov, A. Molinaro, Y. Koucheryavy, A. Iera, and G. Araniti, "Models, Methods, and Solutions for Multicasting in 5G/6G mmWave and sub-THz Systems," *IEEE Communications Surveys & Tutorials*, p. 1, 2023. [Online]. Available: https://ieeexplore.ieee.org/abstract/document/10263616

[33] M. Gapeyenko, A. Samuylov, M. Gerasimenko, D. Moltchanov, S. Singh, M. R. Akdeniz, E. Aryafar, N. Himayat, S. Andreev, and Y. Koucheryavy, "On the Temporal Effects of Mobile Blockers in Urban Millimeter-Wave Cellular Scenarios," *IEEE Transactions on Vehicular Technology*, vol. 66, no. 11, pp. 10 124–10 138, nov 2017.

[34] M. Gapeyenko, V. Petrov, D. Moltchanov, S. Andreev, N. Himayat, and Y. Koucheryavy, "Flexible and Reliable UAV-Assisted Backhaul Operation in 5G mmWave Cellular Networks," *IEEE Journal on Selected Areas in Communications*, vol. 36, no. 11, pp. 2486–2496, nov 2018.

[35] D. Moltchanov, A. Ometov, and Y. Koucheryavy, "Analytical characterization of the blockage process in 3GPP New Radio systems with trilateral mobility and multi-connectivity," *Computer Communications*, vol. 146, pp. 110–120, 2019. [Online]. Available: https://www.sciencedirect.com/science/article/pii/S0140366418309411

[36] A. A. Baktayan, A. Thabit Zahary, and I. Ahmed Al-Baltah, "A Systematic Mapping Study of UAV-Enabled Mobile Edge Computing for Task Offloading," *IEEE Access*, vol. 12, pp. 101 936–101 970, 2024.

[37] M. Banagar, V. V. Chetlur, and H. S. Dhillon, "Handover Probability in Drone Cellular Networks," *IEEE Wireless Communications Letters*, vol. 9, no. 7, pp. 933–937, jul 2020.

[38] M. Salehi and E. Hossain, "Handover Rate and Sojourn Time Analysis in Mobile Drone-Assisted Cellular Networks," *IEEE Wireless Communications Letters*, vol. 10, no. 2, pp. 392–395, feb 2021.

[39] M. K. Somesula, R. R. Rout, and D. Somayajulu, "Contact duration-aware cooperative cache placement using genetic algorithm for mobile edge networks," *Computer Networks*, vol. 193, p. 108062, 2021. [Online]. Available: https://www.sciencedirect.com/science/article/pii/S1389128621001559

[40] City of Melbourne - Open Data Portal, "No Title." [Online]. Available: https://data.melbourne.vic.gov.au/

[41] New York City—Open Data Portal, "No Title." [Online]. Available: https://opendata.cityofnewyork.us/data/
[42] B. Raddwan and I. A. Al-Baltah, "Panda5gSim," 2024. [Online]. Available: https://github.com/yemenlinux/panda5gsim
[43] E. J. Oughton, K. Katsaros, F. Entezami, D. Kaleshi, and J. Crowcroft, "An Open-Source Techno-Economic Assessment Framework for 5G Deployment," *IEEE Access*, vol. 7, pp. 155 930–155 940, 2019.
[44] N. V. Chawla, K. W. Bowyer, L. O. Hall, and W. P. Kegelmeyer, "SMOTE: synthetic minority over-sampling technique," *Journal of artificial intelligence research*, vol. 16, pp. 321–357, 2002.
[45] D. D. Wackerly, W. Mendenhall, and R. L. Scheaffer, *Mathematical statistics with applications*. Thomson Brooks/Cole Belmont, CA, 2008, vol. 7.

BASHEER AMEEN RADDWAN received his B.Sc. degree in electrical and electronic engineering, majoring in telecommunication, in 2003 from Sana'a University, Yemen. Since then, he has worked for Yemen Mobile Company as a manager of core network planning. He received his M.Sc. degree in information technology in 2019 from the University of Modern Sciences in Sana'a, Yemen. He is a Ph.D. student at Sana'a University in Yemen. He focused on the virtualization of mobile core network functions, migration to network function virtualization architecture, and the next generation of mobile networks. He built several private cloud systems that use mainstream systems, such as Ceph storage, OpenStack, and Kubernetes.

IBRAHIM AHMED AL-BALTAH received the B.Sc. degree in statistics and computer science from the University of Gezira, Sudan, in 2007, and the M.Sc. and Ph.D. degrees in software engineering from University Putra Malaysia, Malaysia, in 2009 and 2014, respectively. He is currently an Associate Professor with the Department of Information Technology, Sana'a University, where he has been a Faculty Member, since 2015. He is also the Head of the Information Technology Department. His research interests include green software engineering, resilience software engineering, cognitive software engineering, semantic web, semantic web of things, and semantic data fusion.